ground state and the $P_{3/2}$ neutrons for the first and second excited states. The proton and core capture angular momenta were chosen as 1 and 0, respectively.

The theoretical curves, shown as solid lines in Figs. 3–14, were calculated from the expression

$$\frac{d\sigma}{d\Omega}\alpha \sum_{\substack{\text{final}\\ \text{av initial}}} \left| C_1 \Upsilon_D G_D(K_1) F_D(k_1 R_1) - \frac{\Lambda_2}{\Lambda_1} C_2 \Upsilon_H G_H(K_2) F_H(k_2 R_2) \right|^2,$$

where the notation is similar to that of Ref. 12. The Υ's represent the appropriate sums over the Clebsch-Gordon coefficients. The values of $X=\Lambda_2/\Lambda_1$, R_1 and R_2, chosen to give the best fit to the data, are listed in Figs. 3–14. The numerical calculations were made with the aid of a program written for use on the IBM 7094 computer.

The theoretical results show that the general features of the experimental data can be reproduced by the dual mode theory. Distortion effects have not been explicitly included in the present calculation. Hence, the results presented are subject to possible modification by a more detailed distorted-wave analysis. Such a calculation has been carried out for this reaction at higher deuteron beam energies, the results showing poor agreement between theory and experiment.[2] The most realistic result is to be expected from a calculation which includes both distorted waves and the heavy-particle mode. Efforts in this direction have thus far been unsuccessful.

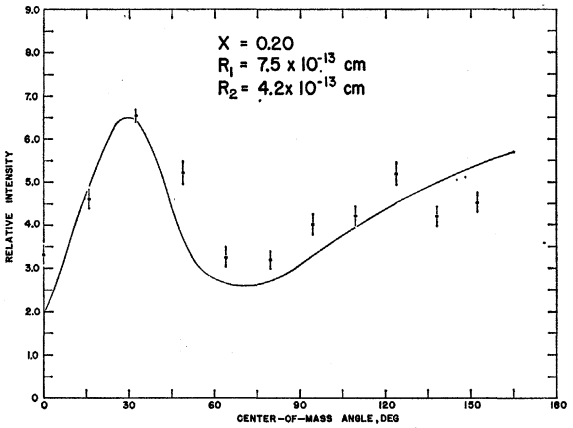

FIG. 14. Second excited-state angular distribution at $E_d=2.5$ MeV.

PHYSICAL REVIEW VOLUME 133, NUMBER 4B 24 FEBRUARY 1964

Energy Dependence of Elastic and Inelastic Scattering from C^{12} for Protons between 14 and 19 MeV*

W. W. DAEHNICK† AND R. SHERR
Palmer Physical Laboratory, Princeton University, Princeton, New Jersey
(Received 4 October 1963)

Differential cross sections $\sigma(E,\theta)$ for elastic and inelastic (4.43 MeV) proton scattering by C^{12} have been obtained as a continuous function of bombarding energy for 15 scattering angles between 15° and 160°. The energy resolution was approximately 200 keV, and the angular resolution was chosen as $\Delta\theta\leq 2°$. The data show several resonance-like variations for $\sigma(E)$, <300 to 500 keV wide for all angles observed. Changes in the elastic and inelastic (4.43 MeV) differential cross sections are closely correlated and are strongest near 15 and 17.6 MeV. In the experiment, use was made of the fact that in a thick target the incident energy is reduced by ionization so that scattering occurs over a range of energies ΔE. Consequently, the energy spectrum of the scattered protons can be used to obtain continuous excitation functions $\sigma(E)$ over the energy interval ΔE. In the present measurements, polystyrene targets of $\Delta E=1.6$ MeV were used. A discussion of the thick-target method is presented. Normalizations and cross checks for the thick-target excitation functions were obtained by conventional thin-target cross section measurements. The latter runs also yielded some cross sections for scattering to the 7.66- and 9.64-MeV states in C^{12}. Scattering to the 0^+, 7.66-MeV state showed strong energy dependence while scattering to the 3^-, 9.64-MeV state showed fluctuations of not more than 15%. The scattering cross sections are compared with optical model calculations by Nodvik, Duke, and Melkanoff,[13] and $C^{12}(p,p'\gamma)C^{12}$ γ-yield measurements by Warburton and Funsten.[24]

I. INTRODUCTION

OF various methods to account for and predict nuclear elastic scattering at intermediate proton energies, the optical model has been most successful. With the aid of 4 to 7 empirical parameters, experimental angular distributions can be fitted, qualitatively correct predictions can be made,[1–4] and often polariza-

* This work was supported by the U. S. Atomic Energy Commission, the Higgins Scientific Trust Fund, and the U. S. Office of Naval Research.

† Present address: Department of Physics, University of Pittsburgh, Pittsburgh, Pennsylvania.

[1] M. A. Melkanoff, J. D. Nodvik, D. S. Saxon, and R. D. Woods, Phys. Rev. **106**, 793 (1957).

[2] A. E. Glassgold, W. B. Cheston, M. L. Stein, S. B. Schulott, and G. W. Erickson, Phys. Rev. **106**, 1207 (1957); A. E. Glassgold and P. J. Kellogg, Phys. Rev. **107**, 1372 (1957).

[3] F. Bjorklund, *Proceedings of the International Conference on the Nuclear Optical Model*, Florida State University Studies No. 32 (Florida State University, Tallahassee, 1959); F. Bjorklund and S. Fernbach, Phys. Rev. **109**, 1295 (1958).

[4] F. Perey and B. Buck, Nucl. Phys. **32**, 353 (1962).

tions and total-reaction cross sections can be predicted with fair accuracy. Attempts have been made to give the optical model a firmer physical basis,[5,6] but usually quantitative work is still phenomenological. Nevertheless, the need of optical model wave functions in DWBA calculations for stripping, inelastic scattering, etc., makes scattering experiments and optical model analysis of elastic scattering interesting, even if the latter cannot be expected to yield a complete explanation of the observed phenomena.[5]

The purpose of the experiment reported here was to investigate in detail the energy dependence of elastic and inelastic scattering of protons from C^{12} rather than their angular distributions at more or less widely separated bombarding energies as had been reported previously.[7–11] Excitation functions were taken in order to determine the location, width, and structure of resonances which were thought to exist. Thick targets were successfully used for this purpose[12] and a detailed analysis of this method is given in the text.

Some of the differential cross sections presented below, and the results of other systematic measurements of $C^{12}(p,p)C^{12}$ were analyzed by Nodvik, Duke, and Melkanoff.[13] With the help of search routines and at the expense of optical model parameter changes from energy to energy, they could fit all C^{12} data between 12 and 20 MeV to almost within the experimental errors. This success in fitting the data is impressive, particularly in view of the general difficulties with light elements.[2] But as might be expected, even with energy variable parameters some small but systematic discrepancies remain. While the effects of compound nucleus formation (N^{13}) are less pronounced between 15 and 20 MeV than at or below 10.5 MeV, even for 19-MeV protons they cannot be neglected.

II. EXPERIMENTAL METHODS

A. Thin Target Measurements

All absolute cross sections reported in this paper were obtained by conventional scintillation-counter spectroscopy. Various thin polystyrene and mylar foils were used as targets. Commercial chemical analysis of these foils showed only minor deviations, in the hydrogen content, from their formulas C_nH_n and $C_{10}O_4H_8$. The target thickness was always chosen to be smaller than 100 keV. In this way, the resolution of the bombarding energy was essentially determined by the energy spread of the protons from the Princeton FM cyclotron. The mean bombarding energy was regulated and measured by a range-energy feedback device.[14,15] The unscattered beam passed through a 0.25 mil mylar foil and was collected in a Faraday cup, which was mounted in high vacuum (2×10^{-5} mm Hg) and equipped with a suppressor magnet. The charge-integrating device has a virtual ground input and is designed to be accurate to better than 1%.

Six NaI counters were mounted inside a 60-in.

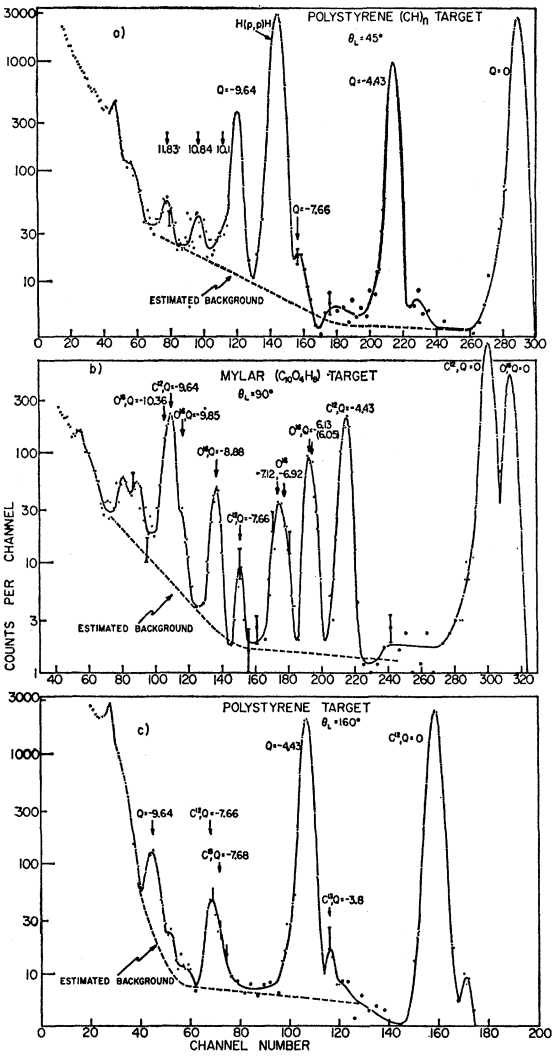

FIG. 1. Typical pulse-height distributions of protons from thin polystyrene (a), (c), or Mylar (b) targets as measured with NaI(Tl) scintillators. The initial proton energy was 18.0 MeV, and peaks are labeled by isotope and excitation energy.

[5] H. Feshbach, C. E. Porter, and V. F. Weisskopf, Phys. Rev. **96**, 448 (1954).
[6] H. Feshbach, Ann. Phys. (N. Y.) **5**, 357 (1958).
[7] I. E. Dayton and G. Schrank, Phys. Rev. **101**, 1358 (1956).
[8] B. B. Kinsey, Phys. Rev. **99**, 332 (1955); **103**, 975 (1956).
[9] R. Peelle, Phys. Rev. **105**, 1311 (1957).
[10] Y. Nagahara, J. Phys. Soc. Japan **16**, 133 (1961).
[11] J. K. Dickens, D. A. Haner, and C. N. Waddell, Bull. Am. Phys. Soc. **7**, 285 (1962); Phys. Rev. **129**, 743 (1963).
[12] W. Daehnick, M. Garrell, R. Wood, and R. Sherr, Bull. Am. Phys. Soc. **6**, 25 (1961). See also A. B. Brown, C. W. Snyder, W. A. Fowler, and C. C. Lauritsen, Phys. Rev. **82**, 159 (1951). The second reference reports the use of thick targets in conjunction with magnetic analysis of the reaction products.
[13] J. S. Nodvik, C. B. Duke, and M. A. Melkanoff, Phys. Rev. **125**, 975 (1962).
[14] G. Schrank, Rev. Sci. Instr. **26**, 677 (1955).
[15] H. Bichsel, Phys. Rev. **112**, 1089 (1958), and private communication. Older range-energy tabulations disagree at 19 MeV by as much as 120 keV.

TABLE I. Experimental cross sections for $C^{12}(p,p)C^{12}$ in the center-of-mass system. (Angles in degrees, differential cross sections in mb/sr.)

E_{LAB} (MeV) \ $\theta_{c.m.}$	16.3°	27.1°	37.8°	48.5°	53.7°	64.2°	74.6°	84.8°	94.9°	104.8°	114.6°	124.3°	133.8°	143.2°	152.5°	161.7°
13.6									19.3	25.1	25.1	21.7	16.3			
8							6.1	12.9	19.5	25.0	23.2	20.2	15.3	10.3	7.4	5.6
14.0							7.2	14.3	20.3	25.1	23.3	19.6	14.4	9.6	7.3	7.1
2							8.7	16.1	22.6	27.3	25.5	20.5	14.6	9.4	7.5	8.4
4							10.8	20.2	26.1	31.4	29.0	22.7	16.5	10.1	8.2	9.2
6							12.2	23.1	28.8	33.4	30.7	24.2	17.5	11.1	7.8	7.6
8	840	387	183	68.4		10.8	12.7	23.5	29.4	32.8	29.2	23.6	16.8	10.9	7.4	5.6
15.0	828	399	183	68.5		10.5	12.6	23.1	28.0	30.6	26.6	21.2	16.0	11.1	8.8	5.8
2	851	407	182	65.3		9.4	11.4	20.5	25.9	28.6	26.0	21.0	16.3	12.2	10.5	9.6
4	853	398	178	65.4		10.5	12.5	21.7	26.5	29.9	27.4	22.7	17.1	11.8	9.6	9.5
6	817	390	186	69.2		11.3	12.5	21.8	28.3	31.2	28.0	22.7	16.5	11.6	9.5	9.8
8	802	394	188	71.5		11.9	12.6	21.7	28.2	31.6	27.9	21.8	15.4	11.0	9.3	10.1
16.0	794	389	190	70.6		12.6	12.7	21.5	28.0	31.2	27.5	21.2	15.8	10.3	9.1	10.2
2	787	401	190	71.7		13.0	13.0	21.3	27.6	29.9	26.2	20.0	13.8	9.5	8.5	10.5
4	796	403	192	72.2		13.3	13.5	21.5	27.5	29.2	25.7	19.2	12.6	8.8	8.1	10.6
6	786	411	194	17.1		13.3	13.7	21.8	26.8	28.4	24.3	17.7	11.9	8.2	7.6	10.2
8	800	415	197	70.3		12.4	13.4	21.8	26.6	27.5	23.2	17.2	11.4	8.2	8.3	10.9
17.0	774	406	185	68.4	36.4	12.4	13.0	21.0	26.3	27.6	23.8	16.9	11.3	7.6	8.1	11.5
2	751	387	182	66.4		12.5	13.1	20.2	24.7	26.8	22.8	17.0	11.5	8.0	8.1	11.2
3	708	385	178	65.6		12.7	13.5	19.6	24.1	25.9	22.8	17.5	11.8	8.6	9.0	11.4
4	718	378	177	63.1		13.0	13.7	19.8	22.8	23.9	20.9	17.0	11.7	9.0	10.2	12.1
5	701		172	63.0		13.3	14.3	20.2	22.1	22.2	19.2	15.4	10.2	9.0	10.9	14.4
6	683	375	169	60.0	33.5	14.3	15.3	20.8	22.4	20.8	16.6	12.8	8.2	8.0	10.7	16.7
7	690	385	172	62.2		14.7	15.5	21.4	22.7	20.6	15.4	10.5	5.9	5.8	8.6	16.5
8	708	395	180	63.6		15.1	15.9	21.6	22.6	21.0	15.4	9.8	5.0	4.37	7.2	14.5
9	714	406	185	65.4		15.0	15.8	21.6	22.2	21.5	16.1	10.0	4.80	3.68	6.5	12.7
18.0	745	418	187	66.6	37.3	15.3	16.0	21.8	23.2	21.9	16.3	10.3	4.79	3.34	6.0	11.5
2	752	422	191	67.1		15.4	16.1	21.7	23.6	21.9	16.8	10.5	4.80	2.82	5.1	10.5
4	749	426	189	67.3		16.0	16.5	21.9	23.8	23.1	18.0	11.1	4.93	2.79	5.2	11.0
6	757	428	188	66.5		16.0	16.6	21.4	23.6	22.9	18.1	12.2	5.2	2.69	5.4	11.8
8	783	440	189	66.4		17.6	17.9	21.0	22.0	22.0	18.7	12.4	5.3	2.40	4.92	12.2
19.0	820	446	191	61.5		18.2	18.2	20.9	20.6		17.4	12.3	6.0	2.90	4.34	10.6
2	857			56.5		18.3	20.0	21.0	18.6	15.9	13.5	10.1	6.4	3.99	4.33	7.7
4	862			52.5												6.3
6	834			50.1												6.2
relative error	3%	2%	3%	2%	8%	3%	3%	2%	2%	2%	2%	2%	2%	4%	3%	3%

scattering chamber described previously[16] and used simultaneously whenever three multichannel analyzers were available. Usually one analyzer was used in a split-memory mode for the recording of the four spectra with the lowest number of counts. Counting losses were held below 2.5%, and corrections were made. Energy resolution of the individual thin NaI detectors could be held to 2% by the selection of phototubes and the use of 0.5-in. cylindrical light pipes. Good resolution was desirable for work with Mylar targets which were used at large angles in order to simultaneously obtain data for O^{16}.[17] Some typical spectra are shown in Fig. 1, and it is apparent that proton groups corresponding to the lowest 3 excited states in C^{12} are usually well resolved. But small contributions from C^{13} (1% abundance) can be seen in places, and the peak for the weakly excited 7.66-MeV level seems to contain appreciable contributions from scattering to C^{12} levels near 7.68 MeV.[18]

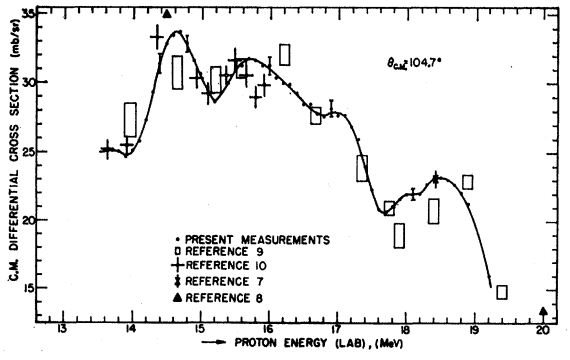

FIG. 2. A comparison of present $C^{12}(p,p)C^{12}$ measurements (connected by solid line) with previously published center-of-mass cross sections at $\theta_{c.m.}=104.7°$. Some typical relative errors are shown for the data reported here. Data from other publications are shown with their absolute errors, if published.

The geometry of the thin-target experiments was such that angular resolutions of $\Delta\theta=\pm 0.5°$ for $\theta<50°$ and $\Delta\theta=\pm 1°$ for $\theta\geq 50°$, or better, were obtained. Very frequently, more than one measurement was made for

[16] J. L. Yntema and M. G. White, Phys. Rev. 95, 1226 (1954).

[17] To be reported in a later article. See also C. B. Duke, Phys. Rev. 129, 681 (1963).

[18] Energies, spin, and parity of levels are taken from T. Lauritsen and F. Ajzenberg-Selove, *Nuclear Data Sheets–Energy Levels of Light Nuclei—May 1962* (National Academy of Sciences–National Research Council, Washington, D. C., 1962), NRC 61-56. This work also contains a very complete set of references to recent $C^{12}+p$ work.

TABLE II. Experimental cross sections for $C^{12}(p,p')C^{12}$ (4.43 MeV) in the laboratory system. (Angles in degrees, differential cross sections in mb/sr.)

E_{LAB} (MeV) \ θ_{LAB}	15°	25°	35°	45°	50°	60°	70°	80°	90°	100°	110°	120°	130°	140°	150°	160°
14.6								7.1	6.1	6.5	8.7	9.5		14.4		
8	58.0	52.0		29.9	25.3	16.5	10.8	7.2	6.0	6.2	7.7	9.7	12.1	13.4	14.3	14.2
15.0		49.3		29.4		17.0		8.0	5.6	5.4	6.7	8.8	11.8	13.2	14.7	14.1
2		46.9		27.1	22.0	16.2	11.5	8.5	6.1	5.4	6.2	8.5	11.9	15.4	17.5	18.4
4	55.3	44.2		25.4		14.7		8.0	6.2	6.4	7.1	9.3	12.0	14.6	16.3	19.6
6		45.1		25.5	21.3	14.8	10.4	7.5	6.0	6.2	7.2	9.5	11.5	13.3	14.7	16.1
8		44.1		25.3		14.2		6.5	5.5	6.0	7.0	8.8	10.5	12.3	12.9	14.0
16.0	50.2	44.4		25.0		13.9	9.0	6.4	5.4	5.8	6.8	8.6	10.0	11.2	12.0	12.8
2		42.6		24.6		13.9		5.9	5.4	5.9	6.6	8.0	9.3	10.5	11.2	12.0
4		41.1	31.7	24.3		13.8	8.7	5.9	5.2	5.7	6.5	7.7	9.0	9.7	10.4	10.8
6		38.3		23.6		13.6		6.1	5.1	5.8	6.5	7.7	8.7	9.5	9.9	10.0
8	38.8	36.6	29.1	23.1		13.9	9.5	6.3	5.2	5.7	6.5	7.9	8.6	9.7	10.5	11.0
17.0	36.9	34.1	27.5	23.4	20.3	14.1	9.5	5.9	4.80	5.1	6.3	7.4	8.5	9.8	10.8	11.7
2		34.3		23.0		13.9		5.8	4.45	5.2	6.1	7.5	8.8	9.8	11.1	12.2
3		32.8	27.3	22.5		13.4	8.4	5.5	4.36	5.1	6.2	7.5	8.9	10.1	11.2	12.4
4		32.4	27.5	21.8		12.8		5.6	4.25	4.85	5.9	7.5	8.7	9.9	10.7	12.3
5		33.0		21.8		12.8			4.25	4.50	5.4	7.0	7.9	9.4	10.3	12.2
17.6	40.2	33.9	26.7	22.5	20.7	13.7	8.8	5.7	4.13	4.14	4.86	6.1	7.3	8.6	9.8	10.9
7		36.1		24.5		14.7				3.95	4.40	5.4	6.3	7.3	8.2	9.4
8		37.3	30.0	24.9		15.1		5.9	4.20	3.80	4.20	5.2	5.9	6.8	7.5	8.5
9		37.0		24.6		15.1	10.0	6.2	4.45	3.90	4.40	5.0	5.8	6.6	7.5	7.8
18.0	38.3	37.6	30.5	24.5	21.2	14.9	9.9	6.2	4.55	4.05	4.55	5.2	5.7	6.6	7.1	7.7
2		34.1		23.6		14.8	10.3	6.3	5.0	4.30	4.65	4.90	5.5	6.2	6.9	7.4
4		32.4	26.1	22.2	19.5	14.0	9.3	6.4	5.1	4.49	4.70	4.87	5.3	5.9	6.5	7.4
6		31.5		21.3		13.1	8.6	5.7	4.90	4.60	4.70	4.85	5.2	5.6	6.2	6.9
8	36.0	32.2	26.3	21.4	18.3	12.7	8.0	5.2	4.64	4.80	4.84	4.91	5.2	5.3	5.9	6.2
19.0	34.2	30.2		20.8		12.5	7.8	4.9	4.45		4.95	4.95	5.2	5.4	5.6	5.7
2	34.0			19.1	17.4	11.5	7.4	5.2	4.34	4.49	4.81	5.0	5.2	5.3	5.7	5.4
4	30.2			18.4			7.2				4.55					5.5
6	34.3			19.2												5.1
Relative error	4%	3%	6%	3%	3%	3%	4%	4%	4%	4%	4%	4%	3%	3%	3%	3%

the cross sections quoted in Tables I and II. In those cases the weighted average of the measurements is given.

While the use of thin targets offers good energy resolution and fairly accurate absolute cross sections, it also presents a number of experimental difficulties, especially if excitation functions are to be obtained. A sequence of measurements at different bombarding energies are related to one another with the aid of energy and beam current monitor readings. This procedure rests on three critical assumptions: (a) The monitors are accurate and reliable, (b) the composition of the target does not change appreciably under bombardment, and (c) counting losses can be corrected for accurately. These assumptions are generally believed to be realizable well enough to keep the monitoring error under 2%. Nevertheless, disagreements of experimental cross sections, even if obtained with similar equipment, often are well beyond the estimated experimental errors. This point is illustrated in Fig. 2 where published $C^{12}(p,p)C^{12}$ cross sections and their quoted statistical plus systematic errors for $\theta_{c.m.}=105°$ are shown[7–10] and compared with the corresponding excitation function presented in this paper. Although the statistical errors may be small, the absolute error of a monitoring system is often difficult to determine. Thus, the combination of different data obtained as angular distributions into a set of excitation functions may lead to false conclusions, especially with regard to finer details if quoted errors are taken at face value.

Reliable excitation functions at a fixed angle have been obtained with high-current accelerators whose energy can be varied accurately and quickly so that the desired information can be obtained in a reasonably short time. Under such conditions, it is possible to study the excitation function in as fine a detail as is desirable. With our FM cyclotron, it is fairly difficult to carry out such measurements to the desired accuracy. Therefore, if excitation functions $\sigma(E)$ could be measured without reliance on any monitor, one would have more confidence in the structure revealed. Our thin-target data are there-

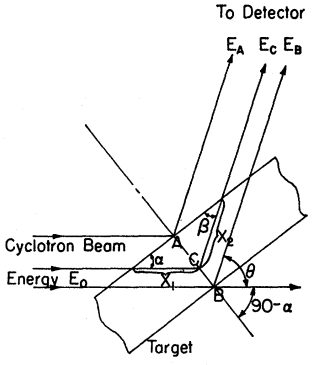

FIG. 3. Illustration of proton paths in a thick target, and definition of symbols used in the text. The three proton trajectories are called "reflected" in the text, since they enter and leave the target through the same surface plane.

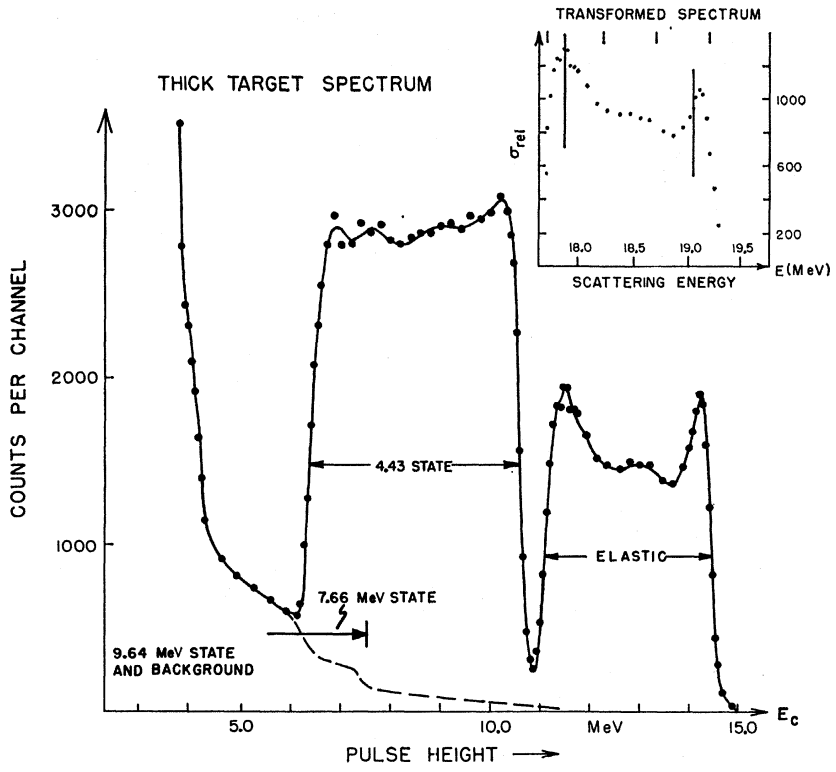

FIG. 4. Pulse-height spectrum of protons scattered from a thick C^{12} target at $\theta_L=140°$. Ground state and first excited state groups are resolved. Total counting time was 10 min at 3×10^{-9} A beam current, and the bombarding energy was $E_0=19.2$ MeV. The insert shows the transformed elastic spectrum, i.e., part of the final excitation curve. Note the close similarity of pulse-height spectrum and excitation curve.

fore compared with excitation functions for $C^{12}(p,p)C^{12}$, which were obtained by the unconventional use of a thick target.[12] As will be shown, the only monitoring required is that of the cyclotron beam energy. Counting loss corrections and beam current integration are not needed. These new $C^{12}(p,p)C^{12}$ measurements were occasioned by Peelle's[9] early data (boxes in Fig. 2) that indicated strong fluctuations in $\sigma(E)$. An independent and more detailed investigation seemed in order.

B. Thick-Target Measurements

In a number of light nuclei the first few states are sufficiently far removed from one another so that even the use of a rather thick target leaves the corresponding groups for the scattered particles well resolved in energy. If the energy loss ΔE of a particle passing through the target is large compared to the available energy resolution in the particle beam and detector, the resulting pulse-height spectrum in the detector can be converted into an excitation function $\sigma(E, \theta=\text{const})$, with $(E_0-\Delta E)<E<E_0$, where $E_0=$beam energy, $E=$scattering energy. This conversion is particularly easy if particles are observed at "back" angles.

A particle elastically scattered at A (Fig. 3) will reach the detector with an energy $E_A=KE_0$, where K is a factor determined by kinematics. A proton scattered at C had a smaller residual energy E before scattering and will reach the detector with an energy $E_C<E_A$. A proton scattered at B will reach the detector with the smallest energy $E_B<E_C<E_A$, because it has to pass through the largest amount of target material (absorber) before and after scattering. Similar arguments hold for inelastic scattering. The energy of the particles incident on the detector is a well-behaved function of the actual scattering energy and vice versa, to the extent that straggling can be neglected.

In Fig. 3, the scattered particles emerge from the back side of the target. Due to the energy losses in the foil, their spread in energy E_A-E_B is considerably greater than the spread in energy of the protons just before scattering, at A and B. This effect improves the energy sensitivity of our scintillation detectors. If the scattered protons emerged from the front face of the target, E_A would be smaller than E_B, and E_A-E_B would be much less than the difference between the energies at scattering, and the effective sensitivity would be considerably reduced. Thus for elastic and inelastic scattering, the present method is useful only for "reflected" particles. In the present measurements, θ was restricted to angles $\geq70°$ since foil surfaces are never perfectly flat. It should be noted that for reactions of the type (α,p), where the proton energy loss is small compared with that of α particles, an excitation curve can be obtained by transmission as well as reflection, so that in principle the entire angular range can be measured.

The energy interval ΔE over which a continuous energy function of elastic scattering can be obtained is limited by the energy of the first excited state. The thickness of the target must be small enough so that E_B is larger than the energy of inelastic protons emerging

from A. In the case of C^{12}, the first excited state is at 4.43 MeV and the useful range ΔE is less than half this value. It is difficult to obtain absolute cross sections with a thick target because of the large angular spread of the beam emerging from the target. However, the reliability of the relative excitation curve over the interval ΔE is limited mainly by statistics. By taking measurements for overlapping intervals ΔE, a complete relative excitation function can be obtained. The absolute scale can then be determined by a thin-target measurement at suitable energy.

The relative excitation functions $S(E,\theta)$ which were obtained covered energy intervals of about 1.6 MeV. E_0 was changed in steps such that there would be good overlap of adjacent measurements. For this experiment, steps of <0.75 MeV were chosen and the regions of good overlap were larger than 0.5 MeV. Normally, more than 5000 counts per 100-keV interval were accumulated so that internal normalization errors due to statistics would be small. Protons were detected with a small (1-in.-diam, 0.1-in.-thick) NaI(Tl) crystal (Harshaw Chemical Company), and pulses from the elastic peak were spread over about 50 channels in a multichannel pulse-height analyzer. A typical thick-target pulse-height spectrum is shown in Fig. 4. The incident beam was defined by 1/8-in. diameter collimators and the scattering angle was restricted to $\Delta\theta=2°$ by a 1/4-in. aperture in front of the NaI crystal. The spectrum shown in Fig. 4 was obtained in 10 min using a beam of about 3×10^{-9} A. The incident energy E_0 again was determined and regulated by the previously mentioned range-energy device.[14] Instantaneous counting rates were kept below 10 000 cps in order to keep pile-up of pulses below 1%. The linearity of the electronics was tested regularly. No corrections were required for the 50 channels of interest.

III. THICK-TARGET ANALYSIS

If the specific range-energy relation in a given absorber is

$$R=R(E), \tag{1}$$

it then follows from Fig. 3 that

$$x_1=R(E_0)-R(E) \quad x_2=R(E')-R(E_c),$$

where E is the energy at scattering and E'=particle energy directly after scattering. Since

$$\frac{x_1}{x_2}=\frac{\sin\beta}{\sin\alpha}=\frac{\sin(\theta-\alpha)}{\sin\alpha}=A(\theta,\alpha), \tag{2}$$

then

$$R(E_0)-R(E)=A(\theta,\alpha)[R(E')-R(E_c)].$$

Now, $R(E)$ for polystyrene is a complicated but well-tabulated function,[19] which for a limited energy interval can be approximated by

$$R(E)=c(E^2+2\gamma E+\delta), \tag{3}$$

where γ, δ, and c are fitting parameters. For the energy interval $5<E<22$ MeV this approximation of R is good to better than 1 mg/cm^2 and the error in the range differences is even smaller.

Thus, using Eqs. (2) and (3), we obtain

$$(E+\gamma)^2+A(E'+\gamma)^2=(E_0+\gamma)^2+A(E_c+\gamma)^2. \tag{4}$$

This relation is quite generally true for Fig. 3 and is based on only one (quite good) approximation, Eq. (3). In a given experiment E_0 and E_c are known and γ and A are constants, but in order to solve for E we still have to know the relation between E and E'. For elastic scattering this is $E'=KE$ where K is given by

$$K=\left(\frac{m}{M+m}\right)^2\left\{\cos\theta+\left(\frac{M^2}{m^2}-\sin^2\theta\right)^{1/2}\right\}^2. \tag{5}$$

From (4) and (5) we find

$$E=(1+AK^2)^{-1}\{[\gamma^2(1+AK)^2+(1+AK^2)\times(E_0(E_0+2\gamma)+AE_c(E_c+2\gamma))]^{1/2}-\gamma(1+AK)\}. \tag{6}$$

For inelastic scattering we must write

$$E'=KE+q'(Q,\theta,E), \tag{7}$$

where Q is the reaction energy, and q' in general a complicated function of Q, θ, and E.

We show in Appendix 1 that $q'(Q,\theta,E)$ is essentially (to order of terms smaller than $mQ^2/4ME$) a function of Q and θ only and can be treated as a constant, thus

$$E'\approx KE+q,$$

where

$$q'\approx q=Q[(M+m\cos\theta)/(M+m)]. \tag{8}$$

Substituting Eq. (8) in Eq. (4), we obtain

$$E=(1+AK^2)^{-1}\{[(\gamma+\gamma AK+AKq)^2+(1+AK^2)\times(E_0(E_0+2\gamma)+AE_c(E_c+2\gamma)-Aq(q+2\gamma))]^{1/2}-(\gamma+\gamma AK+AKq)\}. \tag{9}$$

For brevity, our discussion was limited to reactions like (p,p'), (d,d'), or (a,a'), where the particle type does not change. But similar relations can be derived for (a,p), (p,d), (p,n), and other reactions. Equation (9) reduces to Eq. (6) for elastic scattering (i.e., $Q=0=q$).

If we arrange our geometry so that $\alpha=(180-\theta)/2=\beta$, we have $A=1$ and obtain for inelastic scattering

$$E=(1+K^2)^{-1}\{+[(\gamma+\gamma K+Kq)^2+(1+K^2)\times(E_0(E_0+2\gamma)+E_c(E_c+2\gamma)-q(q+2\gamma))]^{1/2}-(\gamma+\gamma K+qK)\} \tag{10a}$$

and for elastic scattering (with $q=0$)

$$E=(1+K^2)^{-1}\{+[(\gamma+\gamma K)^2+(1+K^2)(E_0(E_0+2\gamma)+E_c(E_c+2\gamma))]^{1/2}-(\gamma+\gamma K)\}. \tag{10b}$$

Equation (9), or the appropriately simplified formulae (6), (10a), or (10b) thus relate the measured energies to the actual scattering energy, and permit us to trans-

[19] M. Rich and R. Madey, UCRL-2301, 1954 (unpublished).

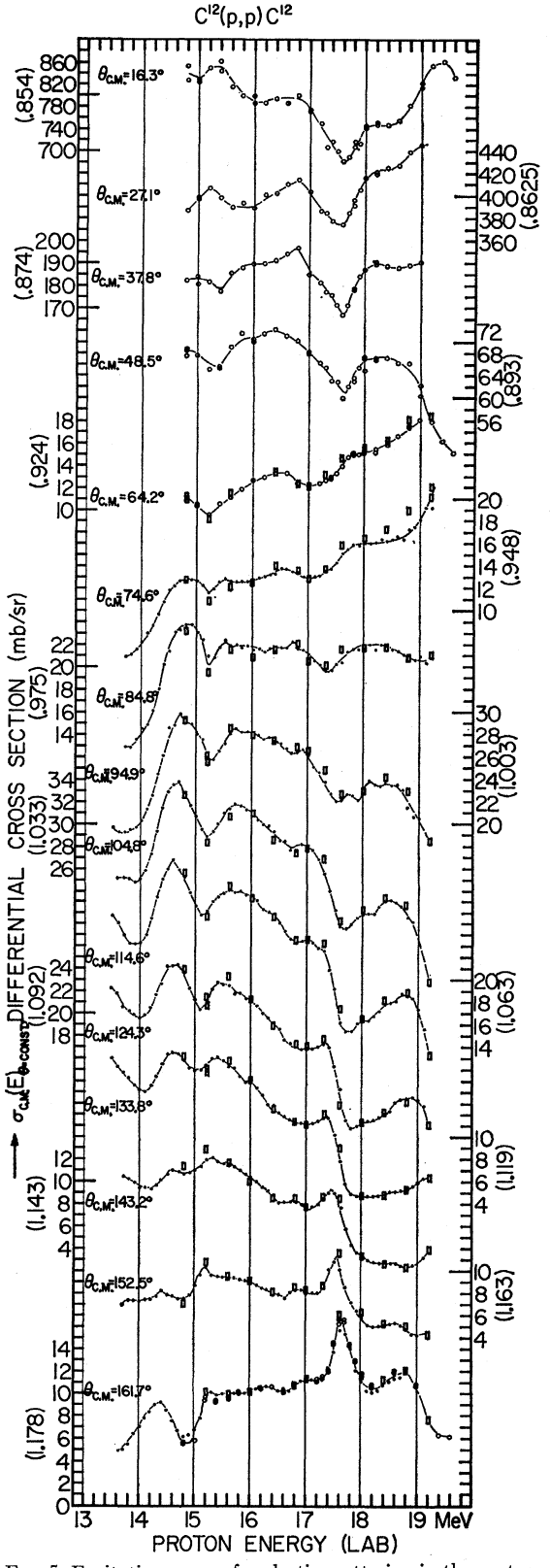

FIG. 5. Excitation curves for elastic scattering in the center-of-mass system. Scales (with suppressed zeros) are in mb/sr. Numbers in brackets were factors used to convert laboratory cross sections into the c.m. values given. Black dots are thick-target data. Open circles are thin-target excitation measurements. Open boxes refer to data obtained as angular distributions for different bombarding energies.

form the measured spectrum $N(E_c)$ into $S(E,\theta)$. In order to transform the numbers N (counts per detector energy channel E_c) into numbers $S(E,\theta)$ proportional to the differential cross section $\sigma(E,\theta=\text{const})$, we recall that for a given range of target matter $dx=dR$, we have a corresponding energy range dE_c.

Thus

$$\sigma(E,\theta)dR\sim S(E,\theta)dR=NdE_c$$

or

$$S(E,\theta)=N\frac{dE_c}{dR}=N\frac{dE_c}{dE}\frac{dE}{dR}. \tag{11}$$

The derivatives dE_c/dE and dE/dR can be obtained from Eqs. (9) and (3) explicitly, and thus the transformation problem is solved.

A. Elastic Scattering Analysis

For elastic scattering analysis, Eqs. (5), (10b), and (11) were used. Transformations were mostly done on an IBM 650 computer after initial experiments and hand calculations had established the usefulness of the method. The transformed spectra (see insert, Fig. 4) were inspected for resolution and a valid region was defined by cutting off about 200 keV from the low- and high-energy ends of the elastic peak in order to eliminate counter resolution effects. The resulting fractions of the excitation functions always showed good agreement with our thin-target data. In the data analysis, background under the elastic peak was neglected.

Overlapping sections of the excitation curves were normalized with respect to each other to yield continuous excitation functions from 13.6 to 19.2 MeV. The entire excitation functions then were normalized at 18.4 MeV to a known absolute cross section.[7] The differential cross sections for elastic scattering so obtained are shown as small black dots in Fig. 5. The open rectangles in Fig. 5 represent our thin-target angular distribution measurements and are included for comparison. The open circles are thin-target data taken as excitation functions, in order to supplement the thick-target data.

B. Inelastic Scattering

At first glance, it may seem that a thick-target investigation of inelastic scattering to the 4.43-MeV state is not very practical since the next level (7.66 MeV) lies fairly close and thus leaves only a very small undistorted range, $\Delta E\approx 1$ MeV, for analysis. Actually, the 7.66-MeV state is so weakly excited in proton scattering that at most it leads to a 5% distortion of the lower-energy end of the broad inelastic peak for the strongly excited 4.43-MeV level, (Fig. 4). We, therefore, analyzed the 4.43-MeV peaks too, using Eqs. (5), (10a), (8), and (11).

Because of both the higher γ-ray and the $Q=7.66$-MeV state background, the thick-target data for inelastic scattering were less accurate than those for elastic scattering. Therefore each transformed inelastic spectrum was normalized separately to the thin-target data it overlapped, as a means to reduce systematic errors due to background. Figure 6 shows the energy dependence of inelastic scattering from the 4.43-MeV level in C^{12}. The black dots again are the thick-target data: 10 to 15 consecutive points were usually obtained in the same run. The open circles are cross sections obtained with conventional thin-target techniques. The dashed lines mainly connect experimental points, and are supposed to approximate the true differential cross sections averaged over energy intervals of about 180 keV.

IV. EXPERIMENTAL ERRORS

A. Energy Errors

For the measurement of excitation functions, the beam energy has to be accurately known and controlled. This was accomplished by a range-energy device[14] the output of which was fed back to the cyclotron magnet control of the Princeton FM cyclotron. For good beam currents ($>10^{-9}$ A on the target) the mean beam energy could be kept constant to $\pm 0.1\%$. For energies below 15 MeV and above 19 MeV, the regulation was somewhat poorer because of very low beam currents. The accuracy of the absolute mean energies quoted depends mainly on the errors in the published range-energy data for aluminum,[15] which are believed to be smaller than 50 keV. In order to recalibrate the energy control device, the $O^{16}(p,\alpha)N^{13}$ resonance at 14.60 MeV[20] was remeasured with stacked foils. Fair agreement with the computed setting was found. We assign probable errors of ± 50 keV to all energy values, but a scale error of ± 100 keV cannot be ruled out.

Comparison of our data with Ref. 10 shows agreement within the combined experimental energy errors, which is 150 keV. In fact, the agreement would be very good if the energy scale of Ref. 10 were increased by 150 keV, or vice versa (see Fig. 2). Comparisons with data of Ref. 7 and Ref. 9 allow no conclusions with regard to the energy calibration.

The energy resolution and spread in bombarding energy for the thin-target data was dependent on the cyclotron beam spread. In the absence of an analyzing magnet, this was found to vary between 110 and 180 keV for the 1/16×1/4-in. collimator. With targets of about 80-keV thickness, the spread in bombarding energy for thin targets was $130<\Delta E<195$ keV. The energy resolution for the thick-target data is somewhat harder to assess. In the typical thick-target spectrum shown in Fig. 4, the broad groups corresponding to scattered protons that left C^{12} in the first excited and ground states are well resolved. The sharpness of the edges gives a good indication of the energy resolution which could be obtained. In the detector spectrum $N(E_c)$, the front edge (of the elastic or inelastic group)

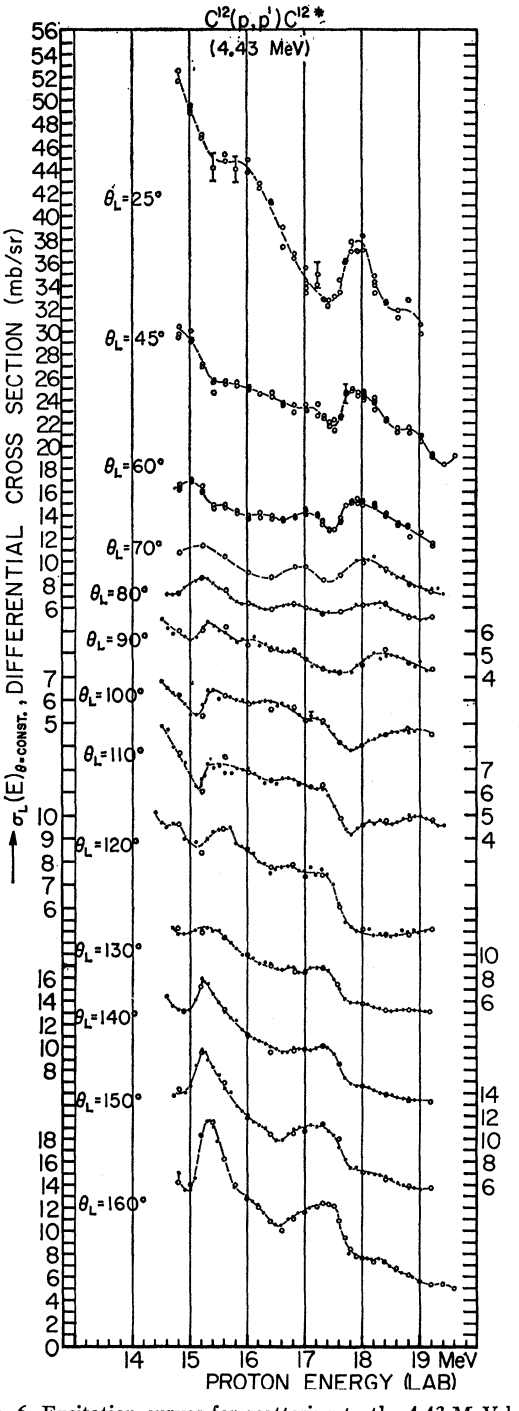

FIG. 6. Excitation curves for scattering to the 4.43-MeV level in C^{12} (laboratory cross sections in mb/sr). Small black dots represent thick-target data which were obtained over ranges of about 1.5 MeV, then normalized to the thin-target measurements (open circles).

[20] H. A. Hill, E. L. Haase, and D. B. Knudsen, Phys. Rev. **123**, 1301 (1961).

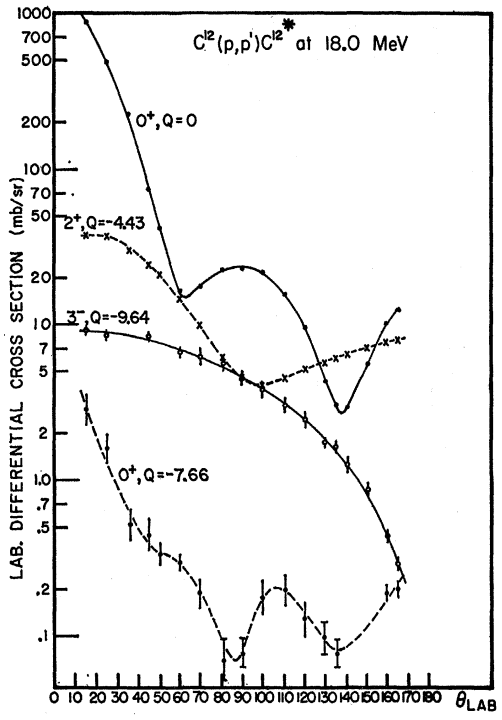

FIG. 7. Typical angular distributions for elastic and inelastic proton scattering at 18 MeV. Relative errors are comparable to the size of symbols unless indicated otherwise. Curves merely connect data points.

rises from 10 to 90% of the full height typically within 330 keV. This is the result of the combination of finite detector resolution (about 2% for 15-MeV protons) and the spread in the cyclotron beam energy (about 180 keV). The latter is in effect reduced by the kinetic factor K. The fall of the low-energy edge of the elastic group occurs within about 370 keV. This resolution is decreased by effects like nonuniformity of the target, straggling, the finite solid angle of the detector, and multiple scattering in the thick target. Appendix 2 gives on estimate of straggling and multiple-scattering effects. The finite solid angle contributes about a 10-keV energy spread which can be neglected. Of the various factors which determine the energy resolution, the most important ones here are the detector resolution and the beam spread. However, in the transformed spectrum the effects of both of them are greatly reduced. The varying absorber thickness, which the protons see on their way out of the thick target, acts like a range-energy analyzer, and a difference of 1 MeV in scattering energy leads to a difference of about 2.45 MeV in detector energy for the geometry used ($\alpha=90-\theta/2$). Therefore, neglecting straggling, the effective detector resolution becomes about 122 keV. The reduction in the effect of the spread in the cyclotron beam can be understood from the following argument. Let us neglect straggling effects after the collision and assume that $N(E_c)$ is measured with a detector of ideal resolution; then a particle detected with E_c must (a) either be a typical particle with incident energy E_0 scattered at C (in Fig. 2) with a residual energy E, the theoretically assumed case, or (b) be a "slow" particle, that had below average energy, say $(E_0-\Delta E_0)$, which was scattered before reaching C, therefore, losing less energy on its way into and out of the target and thus arriving at the detector with E_c, or (c) if the particle had above average energy $(E_0+\Delta E_0)$, it was scattered beyond C losing an extra energy δE_{in} before, and δE_{out} after scattering so that it would still be detected with E_c. Now, the ratio of the energy loss in the target before and after scattering in our symmetric geometry is about 2/3, i.e., $\delta E_{\text{out}}\approx 1.5\delta E_{\text{in}}$, and the actual scattering energy of a particle detected with E_c is $E_{E_0}=E_{\text{theor}}+\Delta E_0-\delta E_{\text{in}}$.

Since $K\Delta E_0=K\delta E_{\text{in}}+\delta E_{\text{out}}\approx(1.5+K)\delta E_{\text{in}}$, we find $E_{E_c}\approx E\pm[1.5/(1.5+K)]|\Delta E_0|$; thus, the effect of the beam energy spread is reduced to $0.65\Delta E_0$ for $K=0.8$ (Eq. 5). For example, an initial beam spread of 180 keV contributed only ≈ 117 keV to the smear in energy resolution in the thick-target spectrum. The predicted ideal energy resolution of $(117^2+122^2)^{1/2}=169$ keV, which does not include straggling effects, is actually better than the width of the cyclotron beam ($\Delta E_0\approx 180$ keV). This is borne out by the sharp rise of the edges in the transformed spectra (see Fig. 4). Straggling and multiple scattering effects are relatively small (Appendix 2) and enter only at the lower end of $S(E)$. It is, therefore, possible to improve the energy resolution in thick-target experiments further by the use of better detectors (for instance, solid state detectors of sufficient stopping power).

Gain shifts in phototube and electronics may lead to an energy resolution poorer than that in Fig. 4. From inspection of the transformed spectra, it is concluded that the energy resolution in the thick target $C^{12}(p,p)C^{12}$ experiment was ≤ 200 keV.

B. Cross-Section Errors

The errors assigned to individual points or excitation curves in the figures and tables are relative errors, which include statistics, errors in background subtraction, counting loss corrections, reproducibility of energy and angular setting, charge, and time readings; i.e., they represent standard deviations for measurements with the same apparatus taken at different times. The quoted errors do not include scale errors due to imperfect calibration of energy and charge measuring devices, nonuniformity of targets, and calibration of zero angle. Such scale errors effect entire excitation functions as a whole, and are of importance if the data presented here are to be compared with absolute measurements by other authors. The energy calibration error has been discussed in the preceding paragraph, and is only important where cross sections vary rapidly with E. The other systematic errors have a more direct bearing on the cross sections.

The angular calibration error is $\pm 0.2°$. The effect of

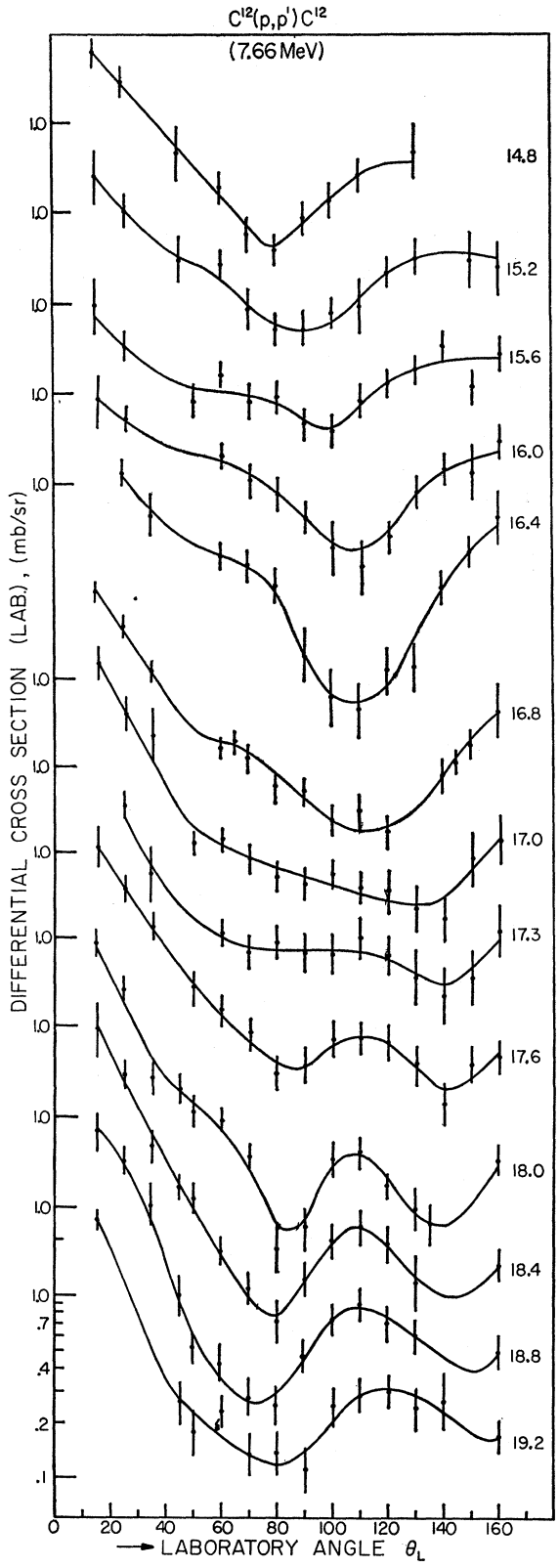

FIG. 8. Approximate angular distributions (in the laboratory system) for 13 bombarding energies for scattering to the 0^+, $Q=-7.656$-MeV state. For this state we find qualitative changes in $\sigma(\theta)$ as a function of energy. The cross sections are subject to large unknown systematic errors due to background and unresolved C^{13} levels. Scales are normally shifted by a factor of 3 with respect to each other.

this error on the cross sections is largest for small angles, and could be as large as 5% for $\theta_L=15°$, but is smaller for all other settings. Effects of target nonuniformity (or decomposition during bombardment) can be serious,[9,10] but are believed small, since small beam currents and 5 different thin targets were used (commerical polystyrene and mylar foils), all yielding absolute C^{12} cross section values that agreed within 2%. The voltage meter of the charge integrator was calibrated with a commercial mercury cell before each run. A systematic error which cannot be excluded is a change of the capacitance of the originally calibrated polystyrene integrating capacitors. This possibility was not investigated further; however, comparison with other published $C^{12}(p,p)C^{12}$ data shows no evidence for a systematic scale error in our data (Fig. 2).

Other effects like counter geometry, multiple scattering in the thin targets, the cut-off of the low-energy tails of peaks for integration, slit scattering, and the 1% abundance of C^{13} in the targets lead to errors smaller than the typical relative errors and were neglected. This procedure very likely is not justified for the scattering cross sections for the weakly excited 7.66-MeV level, where C^{13} contributions could be appreciable. The 7.66-MeV cross sections given, therefore, contain unknown and possibly large systematic errors and should be considered as qualitative information only. Within the rather large errors shown, the 7.66-MeV data are in agreement with data published by Peelle[9] for 16.7-, 17.8-, and 18.9-MeV bombarding energy. The scale error for the excitation functions presented in Tables I and II (not shown) is estimated to be smaller than 5% for forward angles, and smaller than 3% for angles larger than 50°.

V. EXPERIMENTAL RESULTS AND DISCUSSION

Weighted averages of the elastic scattering data shown in Fig. 5 are given in Table I (in the center-of-mass system). The cross sections for inelastic scattering were not transformed into the c.m. system, since the c.m. scattering angle for a given laboratory angle is a function of energy. The weighted averages for scattering cross sections to the 4.33-MeV state are shown in Table II. Data in Tables I and II can be used either as excitation functions or angular distributions. The latter are qualitatively similar over the entire energy region investigated here. Typical angular distributions for scattering to the ground state (0^+) and the first three excited states, $Q=-4.433$, 2^+; $Q=-7.656$, 0^+; $Q=-9.64$, 3^-, are shown in Fig. 7. More elastic angular distributions, including the preliminary data of this article, are shown in Ref. 13. A detailed comparison of the elastic cross sections published here with other data used in Ref. 13 shows excellent agreement with data by Dayton and

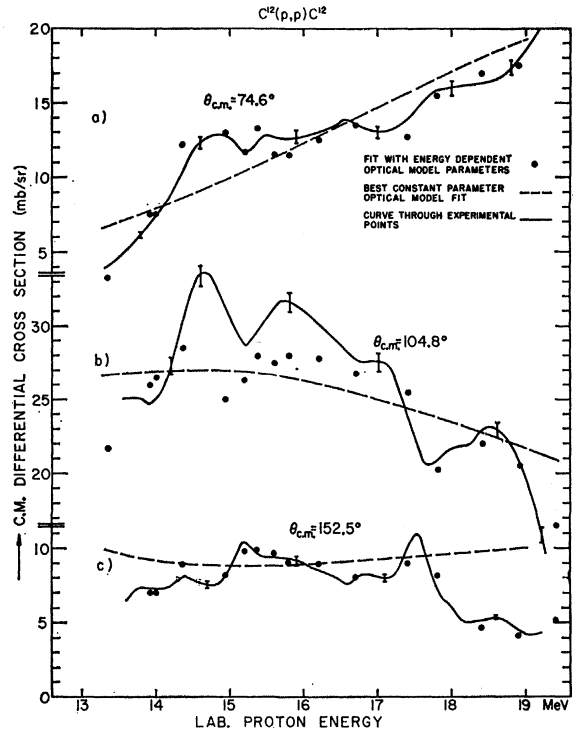

FIG. 9. Comparison of some experimental excitation curves (heavy black lines) with optical model calculations. Dots are best fits with energy-dependent optical model parameters. Dashed lines are best fit with constant optical model parameters. Uncertainty in experimental curves is indicated by error bars.

Schrank[7] for 18.4-MeV protons. Likewise, agreement with Nagahara's data[10] from 14 to 16 MeV is within the combined experimental errors and becomes very good if a slight adjustment in the energy scale is made. Comparison with Ref. 9 for 12 energies between 14 and 19.4 MeV shows agreement to within $\pm 10\%$. This deviation is small; however, it is sometimes twice the sum of the quoted experimental errors. Slightly less accurate angular settings in Ref. 9 and simultaneous difficulties with the uniformity of some targets could explain these discrepancies. It is fortunate that Peelle's data at 16.7, 17.8, and 18.9 MeV agree well with ours, because it is for these energies that cross sections for the 7.66- and 9.64-MeV levels were reported. This permits a good check on our (less carefully measured) data for these levels. Figure 2 would not reveal discrepancies in angular settings or angular resolution since $\theta_{c.m.}=104.7$ corresponds roughly to the center of the second diffraction maximum. This angle was singled out for display, for it would more uniquely than others show differences in the energy and absolute cross-section scales of various papers.

Since inelastic data were obtained simultaneously with the elastic cross sections, no special comparison with other authors is presented. Generally, the 4.43-MeV data are subject to the same errors as the elastic data. For the higher excitation energies, 7.66 and 9.64 MeV, background subtraction and statistics become problems, and the relative errors quoted are generally much higher. Some 7.66-MeV angular distributions are shown in Fig. 8. Here angular distributions as well as excitation functions show strong energy dependence. Scattering to the 9.64-MeV state was not investigated in much detail, but in agreement with Peelle[9] we find no indication for significant changes in the differential cross sections for the investigated energy interval (Figs. 10 and 12).

For an analysis of our elastic scattering data in terms of the optical model, we refer to the work by Nodvik, Duke, and Melkanoff.[13] Fits to the cross sections obtained are surprisingly good, even near bombarding energies that have the appearance of relatively narrow (200 to 500 keV) resonances. Of course, these fits are obtained at the cost of parameter variations that in a somewhat gentler form reflect the resonance-like behavior of the differential cross sections. An optimized constant parameter calculation of the energy dependence in no way reflects the details of the experimental excitation function[21] (Fig. 9).

In Fig. 9, the experimental data are indicated by heavy black lines. The dashed line is the constant parameter fit, and the circles are optimized fits with energy-

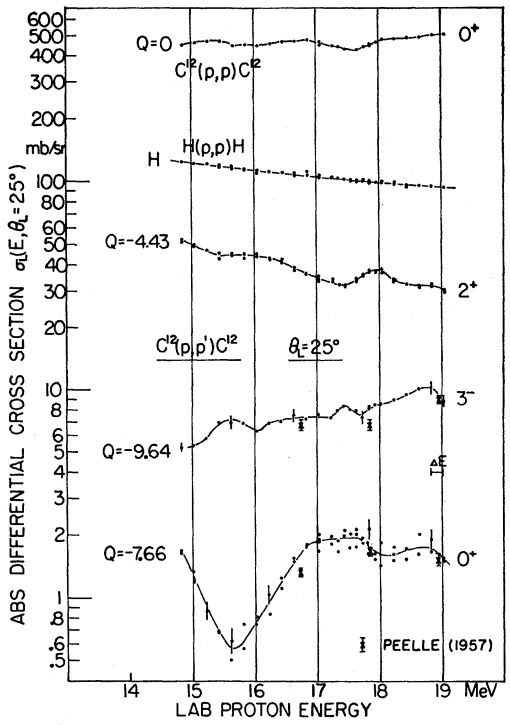

FIG. 10. Logarithmic plot of elastic and inelastic (lab) excitation functions at $\theta_{LAB}=25°$. The scattering of data points for a given energy provides an indication of relative errors. $H(\dot{p},\dot{p})H$ cross sections simultaneously obtained are included to illustrate the extent of systematic errors. Crosses represent data by Peelle (Ref. 9).

[21] The authors are indebted to C. B. Duke for performing this calculation.

dependent parameters.[13] The latter follow the excitation functions fairly well except for $\theta_{c.m.}=104.7°$ where the optical model values are low. Comparison with Fig. 5 in Ref. 13 shows that optical model curves for C^{12} are generally low at the second diffraction maximum.

Phase shift analysis of the best optical model fits shows several interfering l-wave resonances for $14<E<19$ MeV, but no isolated ones.[22] Because of the good optical model fits obtained, a phase-shift analysis of the experimental data is not expected to yield a different result. An attempt was made to fit the inelastic scattering cross sections for the first excited (2^+, $Q=-4.433$) state using a DWBA approach[23] and optical model wave functions from Ref. 13. No satisfactory fits were obtained.

A comparison of Figs. 5 and 6 shows that the resonances for scattering to the first excited and the ground state are closely correlated. A much weaker correlation (if any) exists for elastic scattering and scattering to the 3^-, $Q=-9.64$-MeV state. Figures 10 to 13 compare differential excitation functions for scattering to various final states of C^{12}, for $\theta_{LAB}=25°$, 60°, 110°, and 160°. All differential cross sections show strong variations with energy. Fairly distinct fluctuations are seen at or near bombarding energies of 13.9, 14.4, 14.9, 15.3, 15.6, 16.5, 17.6, 17.9, 18.2, 18.8, and probably 19.4 MeV. These resonances typically seem to have widths from 200 to 800 keV. However, neither their widths nor their

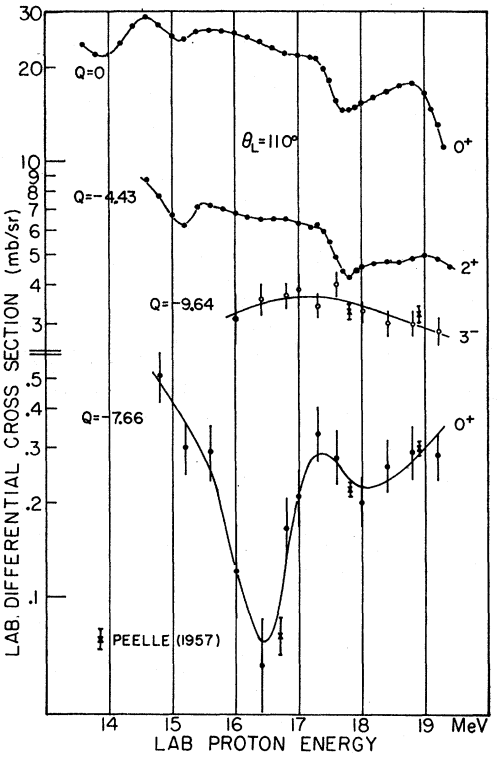

FIG. 12. Comparison of elastic and inelastic scattering at $\theta_{LAB}=110°$. Note the correlation for $Q=0$ and $Q=-4.43$ MeV. Crosses are data by Peelle (Ref. 9).

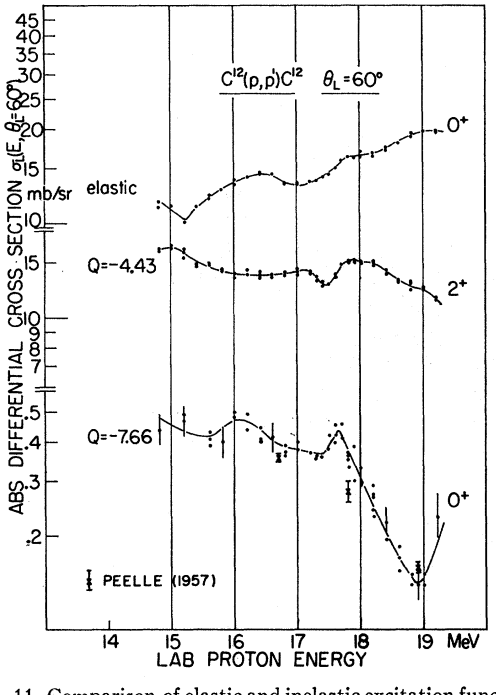

FIG. 11. Comparison of elastic and inelastic excitation functions for $\theta_{LAB}=60°$. Note the broken scales, and the very small cross sections for scattering to the 7.66-MeV level.

[22] C. B. Duke (private communication).
[23] E. Rost (private communication).

locations can be accurately assessed from our scattering data since the resonances generally are not isolated. Figure 14 presents some "total" cross sections for scattering to the ground and first two excited states of C^{12}. These cross sections are approximate in that the elastic curve does not include scattering through angles smaller than 10° (LAB), while for the other curves values for very large and very small angles were found by extrapolation. The total cross sections again show energy dependence, but much less pronounced than that for the differential cross sections. For $Q=0$ and $Q=-4.43$, only the resonance at 17.6 MeV stands out. The 7.66-MeV state scattering shows strong, if broader ($\approx$1 MeV), fluctuations at different energies.

It is of interest to note that the fluctuations at 17.6 and near 19.4 MeV correspond to γ-yield resonances reported at 17.5 ± 0.1 and 19.3 ± 0.1 MeV for the 15.1-MeV γ ray from the $C^{12}(p,p'\gamma)C^{12}$ reaction.[24] Another sharp resonance for the same reaction at 18.1 ± 0.1 MeV, also seen by Warburton and Funsten, is not very apparent in the scattering data, although consistent with our total cross section curves (Fig. 14). Broad resonances for scattering to the 0^+, 7.66-MeV level are seen near 15.6 MeV (Fig. 10), 16.5 MeV (Fig. 12), and 18.8 MeV

[24] E. K. Warburton and H. O. Funsten, Phys. Rev. 128, 1810 (1962); E. K. Warburton and H. L. Berk, Bull. Am. Phys. Soc. 6, 235 (1961).

(Fig. 11). These resonances do not appear strongly for the other states, but could have counter parts in the weak and broad resonances for the 12.7-MeV γ rays for $C^{12}+p$.[24] It is likely that all these fluctuations are due to easily formed states in N^{13}, particularly those near 18.15, 18.7, and 19.8 MeV.[24]

VI. SUMMARY

The energy dependence of elastic and inelastic proton scattering by C^{12} was investigated with 200-keV energy resolution by two independent experimental techniques: Conventional cross section measurements with thin targets, and a novel use of targets 1.5 to 1.8 MeV thick for the measurement of differential excitation function. The latter method was discussed in detail. The two sets of differential excitation functions obtained were in good agreement with each other, and rapid variations of the scattering cross sections for $C^{12}+p$ up to bombarding energies of 19.5 MeV were well established. The widths of the resonance-like fluctuations in the elastic cross sections vary between 200 and 500 keV. These resonances are correlated with those observed for scattering to the 2^+, 4.43-MeV level. Three different resonances in the inelastic scattering to the 0^+, 7.66-MeV state are about 1 MeV wide. Most of these resonances are correlated to γ-ray yield resonances for $C^{12}+p$ reported Warburton and Funsten.[24] There seems to be little doubt that the γ-yield resonances and the scattering cross section fluctuations actually occur at the same energies, and that the latter are compound nucleus

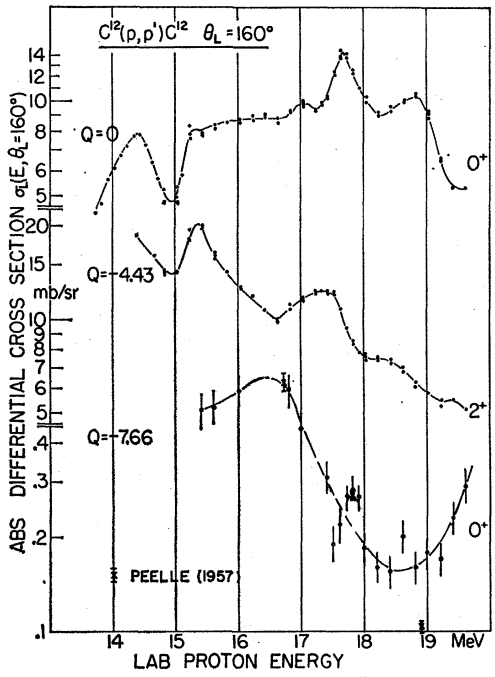

FIG. 13. Comparison of elastic and inelastic scattering at $\theta_{LAB}=160°$. Here variations of differential cross sections with energy are most pronounced. Note the broken scales.

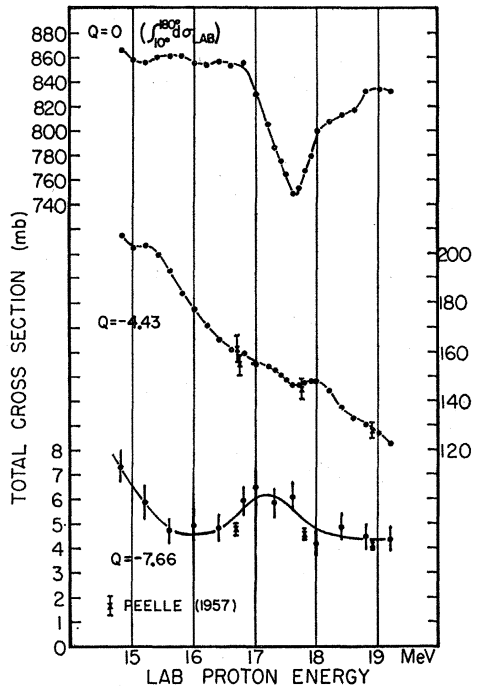

FIG. 14. Approximate total cross sections for scattering to the ground state and the first two excited states of C^{12}. Note suppressed zeros and the limited integration range for the elastic cross sections. All total cross sections show a much smaller percentage of fluctuations than the differential cross sections.

(N^{13}) effects. The constant parameter optical model analysis, of course, did not reproduce any of the details of the cross section variations, nor would it reproduce cross sections that are averaged over one or two MeV. The use of energy variable optical model parameters, however, resulted in surprisingly good fits. It is an intriguing question whether optical model wave functions so obtained actually contain some useful nuclear structure information, or whether the good fits are merely a consequence of the simple angular distribution and the large number of parameters available.

ACKNOWLEDGMENTS

It is a pleasure to acknowledge the assistance of R. Wood and M. Garrell who made the first thick-target measurements and hand calculations. J. Christenson wrote and ran the computer program for the elastic thick-target transformations, and helped extensively in data taking. D. Fong made the thick-target transformations for inelastically scattered protons. We are also indebted to C. B. Duke for making available to us the numerical data of the optical model analysis.

APPENDIX 1: APPROXIMATE FORMULA FOR THE ENERGY LOSS OF ELASTICALLY-SCATTERED PROJECTILES

The exact nonrelativistic relation for the energy E' of projectiles (mass m, initial energy E) inelastically

scattered from nuclei (mass M) is

$$E'=E\left(\frac{m}{m+M}\right)^2\left\{2\cos^2\theta+\frac{M(m+M)}{m^2}\left(\frac{Q}{E}+\frac{M-m}{M}\right)\right.$$
$$\left.+2\cos\theta\left[\cos^2\theta+\frac{M(m+M)}{m^2}\left(\frac{Q}{E}+\frac{M-m}{M}\right)\right]^{1/2}\right\}, \quad (12)$$

where θ is the scattering angle and Q the reaction energy. For elastic scattering, the above formula holds with $Q=0$, and we have $E'_{\text{elast}}=KE$, with K as given by Eq. (5).

We want to write $E'=E'_{\text{elast}}+q'$, and find from Eq. (12) for the difference in energy loss

$$q'=\frac{M}{M+m}Q+2E\cos\theta\frac{Mm}{(M+m)^2}$$
$$\times\left\{\left(1-\frac{m^2\sin^2\theta}{M^2}+\frac{M+m}{M}\frac{Q}{E}\right)^{1/2}-\left(1-\frac{m^2\sin^2\theta}{M^2}\right)^{1/2}\right\}.$$

We always have $m^2/M^2\ll 1$ and $[(M+m)/M](Q/E)<1$ and can expand the square roots in a converging binomial series. Thus

$$q'=\frac{M}{M+m}Q+\frac{mQ}{M+m}\cos\theta+\frac{mQ}{M+m}\cos\theta$$
$$\times\frac{1}{4}\left(\frac{Q}{E}\frac{M+m}{M}-\frac{2m^2\sin^2\theta}{M^2}+\text{smaller terms}\right).$$

We neglect all but the first two terms and find

$$q'=Q\frac{M+m\cos\theta}{M+m}.$$

Since Q is negative, the neglected terms have alternating signs and the maximum error made is

$$|\delta E|<(Q^2/4E)(m/M)|\cos\theta|.$$

For our $C^{12}(p,p')C^{12*}$ experiment with $Q=-4.43$ and $E\approx 16$ MeV, the maximum error is $\delta E<26$ keV, which is smaller than the experimental calibration error.

APPENDIX 2: STRAGGLING IN THICK TARGETS

If targets are thick compared to $E_m=(4m_e/m_p)E_p$, the maximum energy a proton of energy E_p can transfer to an electron, and thin compared to E_p, the distribution function of the proton energy is a Gaussian of width

$$\Delta E=\rho(X)^{1/2}$$

where[25] $X=$ thickness of target in g/cm^2 and

$$\rho^2=\frac{2Cm_ec^2E_m}{\beta^2}\left(1-\frac{\beta^2}{2}\right), \quad \text{with} \quad C=0.150\frac{Z}{A}\left(\frac{\text{cm}^2}{\text{g}}\right).$$

For 16-MeV protons in C^{12}, this yields

$$\Delta E\approx(77600X)^{1/2}(\text{keV}).$$

The maximum target thickness a proton traverses before scattering in the experiment reported here is 0.070 g. Thus $\Delta E=74$ keV. A more typical straggling width is 52 keV. These values are practically energy-independent between 12 and 20 MeV. They have to be added quadratically to the original beam energy spread of about 170 keV which thus is increased by about 10%. Yet, because of the analyzing power of target-absorber plus detector, the effective spread, as we have seen, is reduced by a factor of about 0.65.

The outgoing protons again straggle, and this effect will deteriorate the detector resolution. But even the maximum straggling value of $\Delta E\approx 74$ keV is small compared to the photomultiplier resolution of about 300 keV, and because of quadratic addition yields a negligible decrease in resolution.

MULTIPLE SCATTERING

Multiple scattering in thick targets cannot be negligible and sets a limit to the quality of our angular resolution. A rough estimate of the square of the multiple scattering angle Δ is given by Ref. 26:

$$\Delta^2\approx Z(m_e/m_p)(\Delta E/E)(\text{rad}),$$

where Z is the atomic number, m_e the electron mass, and ΔE the energy loss in the target.

Choosing $\Delta E=4$ MeV and $E=15$ MeV, we find $\Delta^2=0.0284$, $\Delta=\pm 1.6°$ for a very unfavorable case. This does not exceed our geometrical angular resolution of $\Delta\theta\leq 2°$ for thick-target runs.

[25] B. Rossi, *High Energy Particles* (Prentice Hall, Inc., Englewood Cliffs, New Jersey, 1952).
[26] B. L. Cohen, Rev. Sci. Instr. **33**, 85 (1962).